Study of *ab initio* molecular data for inelastic and reactive collisions involving the H_3^+ quasimolecule

P. Barragán, L. F. Errea, A. Macías,* L. Méndez, I. Rabadán,† and A. Riera

Laboratorio Asociado al CIEMAT de Física Atómica y Molecular en Plasmas de Fusión.Departamento de Química, Universidad Autónoma de Madrid, 28049-Madrid, Spain

J.M. Lucas and A. Aguilar

Departament de Química Física. Universitat de Barcelona. CeRQT-PCB. C/ Martí i Franquès, 1. 08028-Barcelona, Spain

(Dated: September 17, 2004)

Abstract

The lowest two *ab initio* potential energy surfaces (PES), and the corresponding nonadiabatic couplings between them, have been obtained for the H_3^+ system; the molecular data are compared to those calculated with the diatomic in molecules (DIM) method. The form of the couplings is discussed in terms of the topology of the molecular structure of the triatomic. The method of Baer is employed to generate "diabatic" states and the residual nonadiabatic couplings are calculated. The *ab initio* results for these are markedly different from the corresponding DIM data, and show the need to consider the third PES.

*Also at Instituto de Estructura de la Materia CSIC, Serrano 113 bis, 28006 Madrid, Spain.

†Electronic address: Ismanuel.Rabadan@uam.es

I. INTRODUCTION

Collision processes between ions and neutrals, atoms or molecules, play an important role in different areas of Physics and Chemistry of low density plasmas and ionized gases [1]. In particular, charge transfer (CT) reactions taking place in condensed phase, where solvent effects are dominant, are nowadays receiving much attention in Biochemistry [2]. However, the study of gas-phase reactions is better suited for arriving at an understanding of the behavior of the kinetics and dynamics of ion-neutral systems, which is essential in order to properly model more complex mechanisms.

As is well known, at low temperatures or collision energies, most atom-molecule reactions evolve adiabatically on a single potential energy surface (PES), and their dynamics, and consequently their kinetics, are essentially controlled by the long-range interaction forces [3] between reactants. On the other hand, ion-molecule CT reactions are essentially nonadiabatic in nature, involving transitions between two or more PES and exploring regions of the nuclear configuration space where diabatic PES cross, the Born-Oppenheimer approximation breaks down, and transitions are most likely to occur.

The study of nonadiabatic reactions needs an accurate determination of both the PESs involved and of the nonadiabatic couplings between the corresponding electronic states. Accurate PESs can be calculated using state-of-the-art *ab initio* quantum chemistry computer codes, although the evaluation of the nonadiabatic couplings is not currently implemented in most packages, except for MOLPRO [4] and the modified MELD [5, 6]. Usually, the *ab initio* calculation only furnishes a pointwise representation of the adiabatic data and both the PES's and their nonadiabatic coupling terms must be fitted to some suitable analytical function before carrying out a dynamical study of the nonadiabatic reaction. For this purpose, it is very useful to know their main characteristics, especially when these are not simple.

Among the less complex nonadiabatic CT reactions are the three-center $(A+BC)^+$ collisions which can lead to simple CT process, with or without nuclear rearrangement. In the present work, we focus on the triatomic system $(H+H_2)^+$, where competition between chemical reaction and CT is possible and which would appear to be the simplest and fundamental reactive system involving only two valence electrons. Its entrance channel can be

either H^++H_2 or H+$H_2{}^+$, which, upon reaction, lead to different product exit channels

$$H^+ + H_2 \rightarrow H + H_2{}^+ \;\; \Delta E = 1.83 \text{ eV} \tag{1}$$

$$H + H_2{}^+ \rightarrow H^+ + H_2 \;\; \Delta E = -1.83 \text{ eV} \, , \tag{2}$$

where processes (1) and (2) are considered to be both purely electron transfer and nuclear reactive arrangements. Also, the isoenergetic reactions ($\Delta E = 0$ eV)

$$H^+ + H_2 \rightarrow H_2 + H^+ \tag{3}$$

and

$$H + H_2{}^+ \rightarrow H_2{}^+ + H \tag{4}$$

have to be considered after a nuclear rearrangement process.

The importance and basic character of the H^++H_2 reaction is probably the reason why this system has attracted so much attention for such a long time, both from the experimental and theoretical points of view. Even restricting our attention to the most recent work, it is unsuitable to give a complete report of the relevant literature on the subject, so that we only consider the most recent and relevant papers in the following section, which nevertheless reads almost as a review of experimental and theoretical contributions. We hope that it is exhaustive enough to show that, to the best of our knowledge, most dynamical treatments are based on DIM surfaces, and that there is little information on the corresponding nonadiabatic couplings. Furthermore, there is practically no information on the accuracy of these couplings with respect to the corresponding *ab initio* results.

In this respect, although *ab initio* energies are known to a spectroscopic accuracy (which is probably unnecessary from the dynamical point of view), what is important is that the *ab initio* PESs and couplings be coherent, that is, stem from the same wavefunctions. This implies that the main characteristics of the evolution of the wavefunctions be accurately reflected in the couplings [7].

Regarding this evolution, the quasimolecule $H_3{}^+$ is peculiar in, at least, three respects. In the first place, there appears a conical intersection between the first two singlet PESs of $H_3{}^+$ at infinite ion-molecule (or molecular ion-atom) separations [8]; this seems to make the construction of diabatic states indispensable rather that an optional step to treat the dynamics. In this respect, while it is well known that there exist different diabatization

methods and that diabatization is not complete, the size and properties of the residual couplings are unknown. Secondly, the appearance of resonance forces between a proton and an H atom gives the molecular data some unique properties that shall be discussed below in Sec. IV. In addition, we have an interplay of resonance, induction and non-additive forces at large distances, and of exchange, correlation and resonance forces at shorter distances, that make the simplicity of the H_3^+ system apparent. These features have not been discussed, in spite of the large literature on the H^++H_2 system. All this justifies the present report of our findings on these points, leaving for future work the dynamical treatment of the process.

The presentation of our new results is split in Secs. III and IV into a report of our methods and data and a topographical description of the coupling surfaces, related to the evolution of the molecular wavefunctions in the different regions. Sec. V is devoted to some characteristics of the adiabatic to diabatic transformation. Our conclusions follow in Sec. VI.

II. HISTORICAL DEVELOPMENT

A. Experimental data

A motivation for the increased interest in $(H+H_2)^+$ CT processes is that vibrational excited states of hydrogen molecules are expected to play a dominant role in fusion energy research, particularly in an energy range of about 1–10 eV, typical of the plasma in the divertor of tokamak devices [9–11]. In this respect, isotopic variants in both impinging ion and neutral target molecules were investigated by Holliday *et al.* [12] using a tandem mass spectrometer. Absolute cross section values were determined as a function of the collision energy as well as the energy distribution of the ionic reaction products.

The first vibrational state-resolved experimental study for the CT reaction (1), in addition to the inelastic collision, was performed by Niedner *et al.* [13] at 30 eV in the laboratory frame. From the comparison of both exit channels, the authors concluded that the CT mechanism involves two steps: an initial vibrational excitation on the lower H^++H_2 potential surface followed by a CT in the exit channel for those vibrationally excited $H_2(\nu' = 4)$ molecules which can overcome the endoergic barrier of 1.83 eV.

More recently, Kusakabe *et al.* [14] reported absolute cross sections for the CT processes between H^+ and H_2, D_2 and other molecules in the 0.2–4.0 keV energy range, using the initial

growth-rate method. The energy dependence of the measured cross sections was compared with available experimental data covering a similar energy range (references are given in [14]), all values being in relatively good agreement among them.

At higher energies, (20–100 keV) McGrath *et al.* [15] studied the collisions of H_2^+ with H, measuring cross sections for the possible processes of dissociation, dissociative capture, target ionization, dissociative target ionization and projectile ionization. In these experiments, the capture process is shown to dominate at the lower energies.

B. Ab initio data for the PES

What is nowadays probably the best calculation for the ground H_3^+ PES is that provided by Cencek *et al.* [16], with an absolute error about 0.02 cm^{-1}, while the best previous calculation, computed with the CISD-R12 [17] method, has error ranging from -3.1 cm^{-1} to 4.3 cm^{-1}. Ref. [16] includes adiabatic and relativistic corrections obtained with the methods of Refs. [18] and [19]. Jaquet *et al.* [20] have then provided an analytical PES which was fitted to the sixty-nine *ab initio* points given in [16], and the computed rotovibronic frequency values for the isotopomers H_3^+ and D_3^+ were found to agree fairly well with the experimental ones.

Prosmiti *et al.* [21] constructed a global PES for the ground state of H_3^+ by fitting a combination of spectroscopic and *ab initio* data; this surface correctly describes the long range part of the potential up to dissociation. Later, Polansky *et al.* [22], improved the accuracy of the previous surface by using additional CISD-R12 *ab initio* data.

More recently, Aguado *et al.* [23] reported a calculation of a PES for the ground state of the H_3^+ system for a large set of points, and using full configuration interaction (FCI) in a (11s6p2d)/[8s6p2d] basis set. The *ab initio* points were fitted to an analytical function which behaves symmetrically with respect to permutations of the hydrogen atoms and covers all regions of the nuclear geometries, the global function error being estimated to be lower than 20 cm^{-1}.

To our knowledge, excited states of (singlet) H_3^+ have only been calculated, within a precision of milihartree, by Errea *et al.* [24]. This precision is amply sufficient for CT dynamical studies at energies $E > 400$ eV.

C. Dynamical calculations

Probably the most important review on the CT H^++H_2 reaction is that of Baer *et al.* [25]. In this paper, the authors performed a three-dimensional quantum mechanical (QM) study of vibrational state-resolved differential cross section for both CT channel and inelastic vibrational excitation. Starting with a 3×3 DIM matrix, the authors used the two lowest singlet DIM-PES [26, 27], correlating with the asymptotic H^++H_2 and H+$H_2{}^+$ channels, to perform a nonadiabatic dynamical calculation on diabatic PES's in the framework of the reactive infinite order sudden approximation (RIOSA) [28–32]. The RIOSA calculations, done at 20 eV in the center of mass (c.m.) framework, were found to properly describe the final vibrational state distribution for H_2 and $H_2{}^+$ as well as their relative branching ratio; also, the theoretical CT differential cross sections showed good agreement with the experimental values, except for the lowest scattering angles.

Because of the difficulties faced up when *ab initio* points of a PES are fitted to an analytical function, Morales *et al.* [33] employed the so-called electron nuclear dynamics approach, that uses a limited electronic basis set instead of analytical potential functions, the full dynamics of electrons and nuclei being considered under the influence of the instantaneous mutual forces. The method describes the nuclei classically while the electronic molecular state is described in a basis of atomic orbitals that move with the nuclei and allows for all possible product channels including CT and nuclear rearrangements. Using a monodeterminantal electronic wave function, the coupled set of dynamical equations is written in terms of the classical Lagrangian including the QM electronic Lagrangian, and solved for a collision energy of 30 eV in the laboratory frame. Results obtained were only partially satisfactory and the authors concluded that a further development of the method is needed in order to explain all details of the dynamics experimentally observed.

A three dimensional QM study of the H+$H_2{}^+(\nu = 0, j)$→ H^++$H_2(\nu')$ reaction has been reported by Last *et al.* [34], employing the DIM-PES's used and discussed in Ref. [25]. This treatment was performed in the framework of the coupled-states approximation, using absorbing negative imaginary potentials that decouple arrangement channels so that only state-to-state non reactive S-matrix elements are determined, and reactive probabilities are calculated from them. Dynamical calculations were done for the reactant molecular ion in the ground vibrational state, $\nu = 0$ and different rotational j states, with the total energy

of the system in the energy range 2.15–2.30 eV. Total CT, reactive CT and non reactive CT processes were considered and the corresponding process probabilities analyzed as functions of the total angular momentum J. For the three types of CT considered, total state-selected cross sections were reported as function of the initial rotational quantum number j; it was found that, at fixed translational energy, the initial value of j has a minor effect on the different process that take place. Furthermore, the authors concluded that results are essentially insensitive to the direction of the reagents' approach.

More recently, Elizaga *et al.* [35] studied the CT processes in H^++H_2 collisions, among others, in the energy range 0.05–6.25 keV, using the sudden approximation eikonal method (SEIKON), which makes use of both the linear trajectories and the sudden approximation. Dynamical calculations were done using *ab initio* data for the PESs as well as for the nonadiabatic couplings. Results obtained were in good agreement with experimental total CT data [36] for energies larger than 500 eV while significant deviations were found at lower E. Later, part of the authors [24], performed calculations where the vibronic part of the collisional wave function was expanded in a set of vibrational states. Results obtained on CT and vibrational excitation compared very well with experimental data for energies larger than 200 eV. In a further contribution, Errea *et al.* [37], using the SEIKON approach, studied the collision $H_2{}^+$+H, both the singlet and triplet subsystems, obtaining good agreement with experimental data of McGrath *et al.* [15], and concluding that the singlet subsystem shows little anisotropy.

Finally, Krstić [38] studied the excitation and CT in H^++H_2 and H+$H_2{}^+$ collisions in the low energy range, 0.6–9.5 eV in the c.m.. Dynamical calculations were performed with the RIOSA approach and using an adiabatic to diabatic transformation of the DIM-PES's, following the procedure of Baer *et al.* [25], including discretized dissociative continua and a modified hamiltonian as discussed in [39]. The calculated CT cross section for H_2, in the ground vibrational state, agrees with the experimental measurement of Holliday *et al.* [12] only in a limited range of energies. Results for different vibrational states of the reactant molecule are also reported and compared with the trajectory surface hoping (TSH) method of Ichiara *et al.* [40]; the authors confirmed the applicability of the TSH method for energies above 10 eV. An exhaustive and detailed study of the inelastic processes leading to dissociation in both H^++H_2 and H+$H_2{}^+$ systems has also been recently reported by Krstić *et al.* [41]. In this paper, an IOSA quantum mechanical study involving a large vibrational basis

set and the corresponding discretized continua is performed in the range of c.m. energies from threshold to 9.5 eV, and for different vibrational states of the diatomic target.

III. *AB INITIO* AND DIM ELECTRONIC CALCULATIONS

A. Potential energy surfaces

In the quasimolecular approach for the H_3^+ reactive system, we have performed adiabatic electronic calculations using the program MELD [5]. Assuming, as in previous work, that at low collision energies only those electronic states of the H_3^+ quasimolecule asymptotically dissociating into channels $H^+ + H_2(X\ ^1\Sigma_g^+)$, $H(1s) + H_2^+(X\ ^2\Sigma_g^+)$ play a major role, our interest is focused on the two lowest PESs.

The *ab initio* electronic calculation has been carried out with a basis set on each proton taken from [42], that consisted of (14s,9p,5d) GTOs contracted to [3s,2p,1d] CGTOs. After the calculation of the corresponding SCF-MO's, a FCI calculation was performed involving 441 configurations. For fixed values of θ, the angle between $\boldsymbol{\rho}$ (the diatomic H–H distance) and $\boldsymbol{R}$ (the distance from the H_2 center of mass to the third nucleus) vectors (see Fig. 1), calculations have been performed in the range 0.5 a.u. $< R <$ 20 a.u. and 0.5 a.u. $< \rho <$ 20 a.u.. For nuclear configurations with C_s symmetry, electronic energies were calculated for $\theta = \pi/12, \pi/6, \pi/4, \pi/3, 5\pi/12$ and for configurations very close to $\theta = 0$ and $\pi/2$ ($C_{\infty v}$ and C_{2v} geometries, respectively), the total number of geometries was about 5000. Moreover, and for the same (ρ, R, θ) geometries considered in the *ab initio* treatment, we also carried out DIM calculations as in [43]. As described in [26], the data are the energy values of $H_2^+(1\sigma_g)$, $H_2^+(1\sigma_u)$ and $H_2(1\sigma_g^2)$ as functions of the internuclear distance, which we have obtained using the method of [44] for H_2^+ and the modified Morse potential fitting for H_2, as in Ref. [45]. Energy values calculated including and neglecting overlap presented no appreciable differences and we have neglected it in our calculations.

The *ab initio* data can be seen in Fig. 2, where only a single value of $\theta = \pi/3$ is given for conciseness, because the results obtained for other attacking angles are qualitatively similar (with some exceptions, see below). As it is known, the two PESs present a conical intersection for $R_{ab} = \rho_0 \approx 2.5$ a.u. and $R_{ac}, R_{bc} \to \infty$. This is due to the fact that the energies of H_2 and H_2^+ coincide for $\rho = \rho_0$, a feature that is well reproduced by the DIM

method. We do not present the corresponding DIM PESs, because they are very similar to the *ab initio* data, and they have been reported several times in the past [8].

We note that Fig. 2 is in terms of Jacobi coordinates (ρ,R,θ), which are suitable to describe the reactants channel, but are not the best for the reaction product channel. Nevertheless, by using the symmetry properties of the system and the data for different θ-angles, one can obtain the relevant information. Fig. 2(a) shows that the ground electronic potential energy of the H_3^+ system, asymptotically correlating with ground state reactants H^++$H_2(X\ ^1\Sigma_g^+)$, is an attractive PES which does not show any potential energy barrier in the entrance valley and leads to a deep well (-0.129 hartree) respect the minimum of the reactants valley (-1.174 hartree), where an H_3^+ adduct has been formed. This adduct can support several bound vibrational states of the angle-fixed triatomic molecule. The location and the depth of the potential well on the ground $^1A'$ PES is angle dependent, with lowest value of -1.3432 hartree for the equilateral triangle geometry ($\theta = \pi/2$) of side $\rho = 1.651$ a.u., in good agreement with the $\rho = 1.650$ a.u. and $E = -1.343100$ hartree values of the most recent *ab initio* calculation of Aguado *et al.* [23]. From the symmetry properties of this minimum, we see that the reactive quasimolecular system can evolve adiabatically into the product valley, asymptotically correlating with $H_2(X\ ^1\Sigma_g^+)$+H^+, provided that the endoergicity of the process is overcome, and without any extra potential barrier. As can also be appreciated in Fig. 2(a), in the strong interaction region of the surface, and after the well, a potential barrier appears at lower values of R and larger values of ρ. However, this barrier or saddle point arises as a consequence of the restrictions done on the attacking θ-angle and would not appear evolving on the ground $X\ ^1A'$ PES along a minimum energy path, or a reaction coordinate evolution where i.e. both θ and ρ are continuously optimized in order to provide the minimum possible electronic energy for a given value of R.

Concerning now the first singlet excited PES ($1\ ^1A'$), it can be seen from Fig. 2(b) that the surface has a repulsive character when R diminishes, leading to a relatively high potential barrier well separating the nuclear configuration region associated with reactants from those for products and correlating both regions asymptotically with the first excited state H+$H_2^+(X\ ^2\Sigma_g^+)$ of the triatomic system. For the considered angle $\theta = \pi/3$ in Fig. 2(b), the barrier appears at -1.002 hartree for $\rho = 4.68$ a.u. and $R = 5.53$ a.u., and lays 0.101 hartree higher than the minimum of the asymptotic atom-molecular ion. This barrier is θ-angle dependent and also appears when following a minimum energy path on the ground $X\ ^1A'$

surface, in our FCI calculation. For a fixed attacking angle (θ) and using ρ and R as representation coordinates, after the barrier is overcome a new $H_3{}^+$ adduct (see Fig. 2) is produced which would correlate to the asymptotical product channel after atomic rearrangements, in a symmetrical way to that described along the entrance channel. However, this minimum appears as a consequence of our restriction on the θ-angle and would not necessarily appear in a treatment of the system following a minimum energy reaction path from (excited) reactants to products. On this $1\ ^1A'$ PES, an adiabatic reactive process would take place for neutral hydrogen atoms and hydrogen molecular ions, both in their ground electronic state, and for the reactants $H^+ + H_2(X\ ^1\Sigma_g^+)$, as a result of an nonadiabatic electronic transition from the ground $X\ ^1A'$ PES of the $H_3{}^+$ supermolecule.

B. Nonadiabatic couplings

We now consider the most important components of the coupling matrix interactions:

$$\partial_Q^k = \langle \Psi_1 | \left. \frac{\partial \Psi_2}{\partial Q} \right|_k \rangle \tag{5}$$

where $\Psi_{1,2}$ stand for the two coupled electronic states, Q for one of the ρ, R, θ coordinates, and k for the fixed remaining coordinates. Calculations were performed for fixed values of the θ-angle, and only $\partial_\rho^{R,\theta}$ and $\partial_R^{\rho,\theta}$ nonadiabatic couplings along ρ and R coordinates, respectively, will be reported.

The *ab initio* couplings were evaluated numerically, as explained in [6]; this method involves the calculation of the delayed overlap matrix elements $< \Psi_i(Q,k) \mid \Psi_j(Q+\delta Q,k) >$. In this work we have used $|\delta| = 10^{-4}$. An important practical difficulty in applying the molecular expansion to many-electron systems is the erratic sign of the molecular wavefunctions Ψ_i, which results in meaningless signs of the dynamical couplings. To solve this arbitrariness, we have implemented [46] an algorithm to automatize the sign coherence of the molecular states Ψ_i, both between successive grid points (Q_j, Q_{j+1}) and in the calculation of the couplings (Q_j, $Q_j + \delta Q$).

With respect to the DIM couplings, we employed the technique presented in Ref. [47]. For each value of the (R, ρ, θ), the $\mathbf{H}$ matrix was obtained at $(Q \pm \delta Q, k)$ and numerical differentiation was used to obtain $\partial \mathbf{H}/\partial Q$, and

$$\partial_Q^k = \bar{\boldsymbol{c}}_1 \frac{\partial}{\partial Q} \boldsymbol{c}_2 = (E_2 - E_1)^{-1} \bar{\boldsymbol{c}}_1 \frac{\partial \mathbf{H}}{\partial Q} \boldsymbol{c}_2 \tag{6}$$

where $\boldsymbol{c}$ are the coefficients of the eigenstates of $\mathbf{H}$. In this case, the sign consistency of Ψ_j was ensured by forcing the leading coefficient of each $\Psi_j(Q_{i+1}, k)$ to have the same sign as that in $\Psi_j(Q_i, k)$.

In Fig. 3(a,b), the evolution of the *ab initio* nonadiabatic couplings between the ground $X\ ^1A'$ and first $1\ ^1A'$ electronic state of the H_3^+ system, as a function of the R and ρ coordinates, is shown for different values of ρ and R. These variations will be examined in the next section. It may be mentioned that the $\partial_R^{\rho,\theta}$ couplings also exhibit a weak θ-dependence. Regarding the $\partial_\rho^{R,\theta}$ couplings, we only observe anisotropy at large ρ values, which will be discussed in Sec. IV C. Of course, if these regions turned out to be explored in the course of a collision process, this would mean that rotational couplings (which are neglected, e.g. in the RIOSA scheme) should also be considered.

As a two-dimensional illustration, isocontour maps for $\partial_\rho^{R,\theta}$ and $\partial_R^{\rho,\theta}$ are given in Fig. 4 for $\theta = \pi/3$, for both *ab initio* and DIM calculations. As can be appreciated, calculated *ab initio* and DIM nonadiabatic couplings look very similar in regions where both ρ and R have values larger than 5 a.u., and the strongest differences appear for lower values. Similar plots are obtained for different values of θ and show qualitatively the same behavior and trends. The overall properties of the couplings are seen from both the contour plots of Fig. 4 and the *locus* of stationary values shown as solid thick lines (ℓ_1, ℓ_2 and ℓ_3 in the figure). Each *locus* is a projection on the (ρ,R) plane of positive or negative ridges of the coupling surface, where nonadiabatic transitions are most likely to occur. *Loci* from *ab initio* and DIM calculations (Fig. 4) are very similar except for $\partial_\rho^{R,\theta}$ couplings at small R values. In fact, the qualitative comparison is so good that it justifies the widespread use of the DIM method in previous work on this system. Nevertheless, as shall be seen, a different matter is that of more refined quantities such as the residual couplings after the diabatization procedure.

Since the characteristics of the couplings reflect the evolution of the electronic wave functions involved [7], their complicated topology will be seen in the next section to follow from geometrical considerations as well as the quantum mechanical interactions between the particles.

IV. TOPOLOGY OF MOLECULAR DATA

Most of the topological properties of both energy and coupling surfaces can be understood from a consideration of the interatomic interactions [7], the fact that two H atoms and an H^+ ion are involved, and the three interatomic distances (R_{ab}, R_{bc} and R_{ac}, see Fig. 1).

Thus, starting in the asymptotic region, where the distances between the ion and both atoms are very large (typically > 12 a.u.), the gap between the PESs is tiny, and induction forces between H^+ and the closest H atom dominate. Since these are attractive, and roughly the same for both electronic states, they contribute little to the energy difference, except when other distances are smaller and a competition with other forces ensues.

When any distance (d) is roughly between 5 and 12 a.u., we have an exceptional situation in that resonance forces dominate. The potential energy that produces these forces decreases like $(1+d)\exp(-d)$, and is responsible for the one-electron bond in $H_2{}^+$ [48]. The forces are very weak, but are attractive when a bonding H–H^+ orbital is formed and repulsive for an antibonding orbital. This gives rise to a pattern of avoided crossings of the quasi-degenerate energy surfaces in the asymptotic region, which considerably affects the dynamical couplings [7].

Next, when d is sizeable but smaller than 5 a.u., exchange forces dominate. The exchange terms are large and negative for the states involved, and roughly decrease like $\exp(-2d)$. Finally at even smaller distances, repulsive interactions come into play, as is well-known [49].

A consideration of the previous features allows to explain most, but not all, characteristics of the surfaces. Here we shall only highlight the main aspects of these characteristics. We take into account that in our figures $R_{bc} < R_{ac}$. The main topological features are due to: the conical intersection at $\rho = R_{ab} = 2.5$ a.u., $R \sim R_{ac} \sim R_{bc} \to \infty$; the trace of this conical intersection, when $R_{bc} \approx 2.5$ a.u., with R_{ab} and R_{bc} finite; and the effect of small forces on quasi degenerate PESs. To explain the effect of these three features, it is useful to distinguish three topological domains I, II, III, as drawn in Fig. 4. Region I stands for explorer points in the (ρ,R) plane where R is larger than ρ and the diatomic fragment (H_a–H_b) is far away from the impinging (H_c) single particle (namely $R_{ab} < R_{bc} < R_{ac}$) and properly describes a situation of a diatom plus an atom. Region II stands for explorer points along the θ-fixed direction where $R_{bc} < R_{ab} < R_{ac}$, and region III describes a nuclear configuration where all

particles are close, when $R_{bc} < R_{ac} < R_{ab}$.

The borders between these domains are given by the straight lines

$$R = 0.5\rho(s\cos\theta + \sqrt{3 + \cos^2\theta}) \tag{7}$$

where $s = 1$ for the border of regions I–II (for $R_{ab} = R_{bc}$) and $s = -1$ for II–III (for $R_{ab} = R_{ac}$). Moreover, the line separating regions I and II is fairly close to the evolution of *locus* ℓ_2 for large values of R. We now pass on to study the three main topological features of the coupling surfaces.

A. Region I

As can be seen from a comparison of Figs. 4(a,b) and Figs. 4(c,d), this region is well described by the DIM method. We first consider the evolution of *loci* ℓ_1 and ℓ_2 in Fig. 4(a,b). We see that, for large R, they coalesce around a value of $\rho = \rho_0 \approx 2.5$ a.u., corresponding to the asymptotical crossing point, or conical intersection, between the ground state potential energy curves of $H_2(X\ ^1\Sigma_g^+)$ and $H_2{}^+(X\ ^2\Sigma_g^+)$. In domain I, it is possible to understand, at least qualitatively, the behavior of the nonadiabatic couplings using standard models [50–53] (see further references in [7]). For this purpose, we can start from a set of two "diabatic" states, such that the nuclear gradient matrix element between them can be considered negligible, and whose asymptotic electronic structure is $H^+ + H_2(X\ ^1\Sigma_g^+)$ and $H + H_2{}^+(X\ ^2\Sigma_g^+)$. We note that, as is well known, strictly diabatic states do not exist for a triatomic [54, 55] and the previous characteristics do not completely define the basis states, but are sufficient for the present descriptive purposes.

We now consider, $R_{ab} = \rho \approx \rho_0$, $R_{bc}, R_{ac} > 5$ a.u.. Since the conical intersection is due to the crossing of the $H_2(X\ ^1\Sigma_g^+) + H^+$ and $H_2{}^+(X\ ^2\Sigma_g^+) + H(1s)$ energies at $\rho = \rho_0$ and $R = \infty$, we can apply the linear model [51, 52] to the "diabatic" energy difference as a function of ρ, which is taken to be of the form $a(\rho - \rho_0)$, with a a constant. Furthermore, the interaction between the "diabatic states" which, as reasoned above, is due to resonance interactions, is exponentially decreasing, and can be modeled by $K\exp(-\alpha R)$ [53] with $\alpha \approx 1$ and K a parameter. There results that

$$\partial_R^{\rho,\theta} \approx s\frac{\alpha}{4}\mathrm{sech}[a(R - R_0)] \tag{8}$$

and

$$\partial_{\rho}^{R,\theta} \approx \frac{-\delta/2}{(\rho-\rho_0)^2+\delta^2} \tag{9}$$

where $\delta = 2K/a\exp(-\alpha R)$, and $R_0 = -1/\alpha\ln(0.5a|\rho-\rho_0|/K)$. In Eq. (8), $s = 1$ for $\rho < \rho_0$ and $s = -1$ for $\rho > \rho_0$.

We can now use this model to explain the structure of the couplings in the I zone. If we consider $\partial_R^{\rho,\theta}$ first, its R-variation is given by cuts of Figs. 4(a,b) parallel to the R axis, as in Fig. 3(a). The intersection between these cuts with *loci* ℓ_1 and ℓ_2 is approximately given in the model by R_0, the location of the maximum (for $\rho > \rho_0$) or the minimum (for $\rho < \rho_0$) of the coupling. From the model we see that the corresponding variation with ρ of $\partial_R^{\rho,\theta}$ yields both a maximum and a minimum (due to ρ-dependence of R_0).

A similar argument can be used to explain the evolution of the ρ-coupling matrix elements for a fixed value of R inside the considered region I in Fig. 4(c,d). These coupling matrix elements shown a Lorentzian profile as a function of ρ, peaked at $\rho = \rho_0$ [see Fig. 3(b)], which becomes more and more narrow as R increases, tending to a Dirac-δ function in the asymptotic limit $R \to \infty$, as explained by Baer [56]. When the explorer point moves inside region I to lower values of the internuclear distances, where exchange forces dominate, the model is too naive in that ρ_0 should depend on R and, accordingly, the evolution of the ℓ_1 *locus* departs from the linearity obtained for large values of R.

B. Border I–II

A second region of interest, concerning PES and coupling matrix elements, is the frontier between regions I and II (in Fig. 4). In this region of internuclear distances, the PESs are practically degenerate, and also practically degenerate with the energy of the third state. In such a situation, any small interaction can give rise to configuration mixing, and therefore to sizeable nonadiabatic couplings. From Figs. 4(a,b,c,d) we see that both $\partial_R^{\rho,\theta}$ and $\partial_{\rho}^{R,\theta}$ show a ridge (ℓ_2 *locus*) when $R_{ab} = R_{bc}$ and R_{ac} range between 5 and 12 a.u.. There, small resonance forces dominate, while polarization and exchange forces play a secondary role. Comparison between Figs. 4(a,b) shows that $\partial_R^{\rho,\theta}$ is similar for the DIM and *ab initio* data, but Figs. 4(c,d) do not give a similar agreement for the $\partial_{\rho}^{R,\theta}$ coupling; in fact, the *ab initio* coupling is about twice as large as the DIM one, which led us to study this matter in detail.

The physical structure of the DIM states in the I–II border can be understood from a

consideration of two-body forces in a valence-bond picture of orbital products. Resonance forces between H^+ and the H atom that is closest give rise to bonding (and anti-bonding) two-center orbitals. When the explorer point moves along a path in the neighborhood of the border, geometrical considerations using

$$\begin{cases} R_{ab} &= \rho \\ R_{bc} &= (R^2 \sin^2\theta + (R\cos\theta - \rho/2)^2)^{1/2} \\ R_{ac} &= (R^2 \sin^2\theta + (R\cos\theta + \rho/2)^2)^{1/2} \end{cases} \tag{10}$$

allow to explain the corresponding changes in the form of the wavefunctions, as the bonding orbitals are formed between different pairs of atoms, and thence the form of the couplings with the maximum at the border.

This situation is slightly complicated, at larger distances, by the competition with induction forces, but the issues are still predictable using back-of-the-envelope arguments. In particular, the interplay of attractive and repulsive resonance forces with (always attractive) induction forces results in sharp avoided crossings between the second and third PESs, which produce highly peaked couplings there. We do not illustrate these considerations because the DIM model turns out to be too simple in the I–II border region. A detailed study of the configurations involved shows that the *ab initio* wavefunctions have a more complicated variation than the DIM ones, because in the former, small non-additive interactions (triple dipole) and charge transfer (ionic structures) are at play, and this results in more complex mixing of the valence bond structures than that predicted by the DIM model, and much stronger nonadiabatic couplings of the two states considered here with the third state that is almost degenerate with them. Furthermore, since the molecular data are not symmetrical in the R and ρ Jacobi coordinates, see Eq. (10), these additional mixings turn out to affect more the $\partial_\rho^{R,\theta}$ coupling than $\partial_R^{\rho,\theta}$.

C. Region III

In the third region of interest, there are also appreciable differences between the *ab initio* and DIM results, as can be seen in Fig. 4. The topology in this region is more complicated than the previous ones, because it requires the consideration of different θ angles. An indication of this is given by the strong θ dependence of energies and couplings (Fig. 5). The

(simpler) DIM method provides the means to partially understand the physical situation, and the complications leading to the *ab initio* data can be seen from Figs. 4(a,c).

The evolution of *locus* ℓ_3 in Fig. 4 can be considered as a "shadow" of a second conical intersection for $R_{bc} = \rho_0$ with the other two distances finite (rather than infinite, that would yield a true intersection). This condition yields the parametric equation for an ellipse:

$$\begin{cases} \rho - 2R\cos\theta &= 2\rho_0 \cos t \\ R &= \rho_0 \sin t / \sin\theta \end{cases} \tag{11}$$

where θ and t are the angles shown in Fig. 1. The location of this ellipse is indicated in Fig. 5 with a green line. As the explorer point gets near the ellipse, the conical situation is approached, so that the two PESs become closer, and the couplings larger. This situation is, of course, not reached, except in the limit $\theta = 0$, $\rho \to \infty$.

Furthermore, as the explorer point travels along the ellipse, ρ increases up to a value $\rho_{\max} = 2\rho_0/\sin\theta$ for $t = \pi/2 - \theta$, and then recedes from this situation at larger t, crossing the II–III border. As a result we have a sign change in the coupling (Fig. 5), just as when one goes along l_1 to $R \to \infty$ and then passes to the l_2 locus in Fig. 4(b).

All these considerations are the more valid the smaller the value of θ, while for θ close to $\pi/2$, the three distances between the atoms are comparable and the situation is unrelated to a conical intersection. On the contrary, as θ decreases, the relevant distances R_{ab} y R_{ac} become larger, so that the model becomes more accurate, and the *locus* tends to coincide with the ellipse. We finally note that similar arguments allow to relate the topology of the PESs in Fig. 2 in regions I and II.

With respect to the *ab initio* data, Figs. 4(a) and 4(b) show that *ab initio* $\partial_R^{\rho,\theta}$ couplings in region III are very similar to the DIM ones, so that the previous explanation also applies. In Figs. 4(c) and 4(d), we see that differences appear for $\partial_\rho^{R,\theta}$ couplings, which we attribute to the fact that for the range of internuclear distances involved, electronic interactions are very strong, and need a proper and accurate description of the three center exchange and correlation forces, which are better described by MELD through the FCI wavefunctions. These interactions also result in stronger nonadiabatic couplings with higher lying states. In particular, it may be noted, although we shall not illustrate it here, that at small distances, the second and third state present a conical intersection in the (R,θ) plane for any fixed ρ and at $\theta = \pi/2$. Hence, the corresponding couplings are singular there [57]. This feature

appears in both the DIM and *ab initio* results, although the third state in the *ab initio* results differs from the DIM one, whose energy lies a little higher.

V. RESIDUAL COUPLINGS IN THE ADIABATIC TO DIABATIC TRANSFORMATION

CT reactive and non reactive processes are controlled by nonadiabatic couplings and the dynamics and the kinetics of the process can be only understood by properly considering these couplings. It is well established [25] that dynamical calculations including the corresponding nonadiabatic couplings can lead to numerical instabilities so that a previous adiabatic to diabatic transformation is usually preferred. Such a transformation would partially remove the nonadiabatic couplings, and transfers them to diabatic couplings through the corresponding electronic non-diagonal hamiltonian matrix $\mathbf{W}$. We stress that, since the removable part of the couplings contains the singular interaction at the conical intersection [57], such partial transformation is indispensable in the present case.

A dynamical study would then employ the diabatic energies and the hamiltonian coupling, and most probably neglect the residual nonadiabatic couplings issued from the transformation. Since the diabatic hamiltonian matrix elements are similar for the *ab initio* and DIM data, they will not be discussed here. A different matter, however, concerns the size of the residual couplings and this is the subject of the present section.

Although different diabatization methods have been proposed [54, 56], we shall follow the procedure described by Baer (see [56] for details). An orthogonal transformation $\mathbf{W} = \mathbf{A}^t\mathbf{H}\mathbf{A}$ is performed where the non-diagonal W_{ij} elements are the diabatic hamiltonian couplings, and the diagonal W_{ii} matrix elements are the diabatic potential surfaces. For each fixed value of the θ angle, the $\mathbf{A}$ matrix takes the simple form [56, 58],

$$\mathbf{A} = \begin{pmatrix} \cos\alpha & \sin\alpha \\ -\sin\alpha & \cos\alpha \end{pmatrix} \tag{12}$$

with the transformation angle α given by [56]:

$$\alpha(R,\rho) = \alpha_0 + \int_{R_0}^{R} \partial_R^{\rho,\theta}(R',\rho)dR' + \int_{\rho_0}^{\rho} \partial_\rho^{R,\theta}(R_0,\rho')d\rho' \tag{13}$$

Since the diabatization method is not exact, there remains the residual couplings:

$${}^{\mathrm{d}}\partial_R^{\rho,\theta} = 0 \quad ; \quad {}^{\mathrm{d}}\partial_\rho^{R,\theta} = \partial_\rho^{R,\theta} - \frac{\partial\alpha}{\partial\rho} \tag{14}$$

and these are shown in Figs. 6(a,b) for the DIM and *ab initio* methods; as far as we know, this is the first report of a calculation of residual couplings for a triatomic system. In Eq. (13), $\alpha_0 = \alpha(R_0, \rho_0)$ can be taken to be 0 and ρ_0 and R_0 are suitable points such that the numerical integrations involved in Eq. (13) are easily performed; for this, the point (R_0,ρ_0) should be far from any *locus* of Fig. 4, as discussed in Sec. IV. For instance, one can choose points in region I, where no contours appear in Fig. 4, so that couplings are very small, and in our calculation we chose $R_0 = 10.0$ a.u. and $\rho_0 = 1.0$ a.u.. Another technical point is that when the integration path crosses a *locus*, the number of integration nodes must be correspondingly increased. This point becomes crucial with respect to *loci* ℓ_1 and ℓ_2 of Fig. 4, in the neighborhood of the singular coupling.

We see in Fig. 6 that the outcome for both methods is dramatically different. For the DIM method, residual couplings turn out to be practically negligible throughout and this justifies a limitation to a two-state dynamical treatment in the frame of this method. With respect to *ab initio* residual couplings, we first note, that the quasi-singular peak also disappears. It may be mentioned, in this respect, that this canceling out of the two delta-like peaks in $\partial_\rho^{R,\theta}$ and $\partial\alpha/\partial\rho$ in Eq. (14) is not without numerical difficulties, unless an extremely fine grid or points is employed, and the unavoidable irregularities in our data have been smoothed out in the figures. Secondly, we find that, in contrast with the DIM result, the *ab initio* residual coupling is almost as large, and sometimes even larger than, the original nonadiabatic one. Such a finding is very important, since it would seem to invalidate a two state treatment using *ab initio* data. Its origin can be traced to both the different behavior of $\partial_\rho^{R,\theta}$ and $\partial_R^{\rho,\theta}$ in the I–II border and the III region of Sec. IV, as well as to the importance of the third state in this region.

For this purpose, from Eqs. (13) and (14), one can obtain:

$$ {}^{\mathrm{d}}\partial_\rho^{R,\theta} = \int_{R_0}^{R} \left(\frac{\partial}{\partial R} \partial_\rho^{R,\theta} - \frac{\partial}{\partial \rho} \partial_R^{\rho,\theta} \right) dR' \tag{15} $$

We can then adapt Baer's arguments [56] on the accuracy of the diabatization procedure in the limit of a complete basis, by taking the three-state manifold as sufficiently complete, and using closure:

$$ {}^{\mathrm{d}}\partial_\rho^{R,\theta} = \int_{R_0}^{R} \left[\langle \Psi_3 | \frac{\partial \Psi_1}{\partial R} \rangle \langle \Psi_3 | \frac{\partial \Psi_2}{\partial \rho} \rangle - \langle \Psi_3 | \frac{\partial \Psi_2}{\partial R} \rangle \langle \Psi_3 | \frac{\partial \Psi_1}{\partial \rho} \rangle \right] dR' \tag{16} $$

This expression relates the residual coupling ${}^{\rm d}\partial_{\rho}^{R,\theta}$ to the nonadiabatic interaction between the first and second with the third state, which we have stated to be much larger for the *ab initio* data that for the DIM results both in the I–II border and in region III. In particular, the analysis applies to the I–II border in the large ρ region where *ab initio* couplings to the third state are about twice as large as the DIM ones (Section IV). When in expression (13) the path crosses the I–II border for large R, ρ, there results large residual couplings for large ρ in Fig. 6. Incidentally, the same reasoning explains the oscillations in the asymptotic structure of the couplings as arising from couplings with the third state, as mentioned in section IV. The same oscillatory features appear, to a lesser extent, for the DIM data, for which these couplings are more localized.

In summary, we find that with the choice of path in Eq. (13) –which is first parallel to the ρ-axis and then to the R one– residual couplings are much larger for the *ab initio* than for the DIM data, and this can be traced to the size of the couplings with the third state, along the path. Moreover, we also found that, unlike the corresponding DIM data, the *ab initio* residual couplings are strongly path-dependent. Form Ref. [55] (using Stokes' theorem), the difference between the residual couplings obtained from two different paths is given by the integral of the integrand of Eq. (15) over the surface enclosed by the two paths. We have explicitly checked that this difference is far from negligible, by using a second path that is first parallel to the R-axis and then to the ρ one, so that the surface is a rectangle. Accordingly, the *ab initio* states obtained by a two-state diabatization are not unique.

The present conclusions on the contribution and role of the different excited electronic states in the dynamics of the $(H+H_2)^+$ system, in this case the third state, agree qualitatively with the statement of [59] on the participation of three electronic states on the proper description of the dynamics of the system using adiabatic DIM surfaces. In fact, we see that this is enhanced for the *ab initio* results, since we have seen that the DIM method underestimates the nonadiabatic couplings to the third state involved.

VI. CONCLUDING REMARKS

In this paper we have presented a study of the molecular data required to treat reactions (1–4) obtained with both DIM and *ab initio* methods. As stressed in the introduction and Sec. II, the $H_3{}^+$ system is sufficiently simple and important to warrant the large amount

of dynamical studies carried out both from the experimental and theoretical sides. Since time seems to be ripe for a nonadiabatic dynamical treatment of the reaction, a point of interest is the accuracy of the widely used DIM method in both the description of the PESs and nonadiabatic couplings. Another point is to what extent this description can be restricted to a two-state manifold of electronic wavefunctions. Our report aims at providing a study of these points that can be used in future works, as well as a detailed topographical analysis of coupling and energy surfaces for the lowest two electronic states of $H_3{}^+$.

We have seen, in particular, that the PESs corresponding to the first two states that would be involved in the treatment are well described by the DIM method. A similar situation is found for the nonadiabatic couplings in the vicinity of the singularity at the conical intersection of the surfaces. However, we found that elsewhere, one of the couplings ($\partial_\rho^{R,\theta}$) is markedly different, and this could lead to important consequences on the dynamics of $H^+ + H_2$, even at relatively low collisional energies.

We have performed a diabatization procedure using the well-known method of Top and Baer [60], and found that residual nonadiabatic couplings, though nonsingular, are far from negligible for most nuclear geometries. In principle, one would have expected our "diabatic" states to be a good basis to treat the dynamics, especially if both hamiltonian and residual nonadiabatic couplings are taken into account in this treatment. However, at the present stage, it is not clear that this is so because the large *ab initio* residual couplings are an indication that interactions with the third state (at least) should also be taken into account. This is a point that we have explicitly checked by calculating the couplings with the third state, although a description of these data is outside the aim of the present paper. Nevertheless, our conclusion on this point should not be unnecessarily negative, since it is not obvious that the abovementioned interactions would have a strong influence in the accuracy of the cross sections for reactions (1) to (4). Because of this, it is difficult to definitely assess the importance of our findings on the shortcomings of the two-state basis set without performing a dynamical treatment, and work is in progress along these lines.

ACKNOWLEDGMENTS

This work has been partially supported by DGICYT projects No. BFM2000-0025 and FTN2000-0911. I.R. acknowledges MCyT for a "Ramón y Cajal" contract. J.M.L. and A.A. also thanks support given by the Spanish Ministry of Science and Technology project No.

BQU2001-3018 and the Generalitat de Catalunya-DURSI project No. 2001SGR 00041.

[1] D. L. Lambert, Phys. Scr. **T47**, 186 (1993).

[2] V. A. Shuvalov and U. Heber, Chem. Phys. **294**, 227 (2003).

[3] J. Troe (John Wiley & Sons, Inc., 1997), vol. 101 of *Advan. Chem. Phys.*, p. 819.

[4] *MOLPRO is a package of ab initio programs written by H. J. Werner and P. J. Knowles, with contributions from J. Almlöf, R. D. Amos, M. J. O Deegan, S. T. Elbert, C. Hampel, W. Meyer, K. Peterson, R. Pitzer, A. J. Stone, P. R. Taylor and R. Lidth, M. E. Mura, and T. Thorsteinsson.*

[5] E. R. Davidson, in *MOTECC, Modern Techniques in Computational Chemistry*, edited by E. Clementi (ESCOM Publishers B. V., Leiden, 1990).

[6] J. F. Castillo, L. F. Errea, A. Macías, L. Méndez, and A. Riera, J. Chem. Phys. **103**, 2113 (1995).

[7] A. Riera, J. Mol. Spec. **300**, 93 (1993).

[8] M. Baer, Adv. Chem. Phys. **82**, 187 (1992).

[9] A. Y. Pigarov and S. I. Krasheninnikov, Phys. Lett. A **222**, 251 (1996).

[10] S. I. Krasheninnikov, A. Y. Pigarov, T. K. Soboleva, and D. J. Signar, J. Nucl. Mater **241**, 283 (1997).

[11] R. K. Janev, Contrib. Plasma Phys. **38**, 307 (1998).

[12] M. G. Holliday, J. T. Muckerma, and L. Friedman, J. Chem. Phys. **54**, 1058 (1971).

[13] G. Niedner, M. Noll, J. P. Toennies, and C. Schlier, J. Chem. Phys. **87**, 2685 (1987).

[14] T. Kusakabe, K. Asahina, J. P. Gu, G. Hirsch, R. J. Buenker, M. Kimura, H. Tawara, and Y. Nakai, Phys. Rev. A **62**, 062714 (2000).

[15] C. McGrath, M. B. Shah, P. C. E. McCartney, and J. W. McConkey, Phys. Rev. A **64**, 062712 (2001).

[16] W. Cencek, J. Rychlewski, R. Jaquet, and W. Kutzelnigg, J. Chem. Phys. **108**, 2831 (1998).

[17] R. Rhse, W. Kutzelnigg, R. Jaquet, and W. Klopper, J. Chem. Phys. **101**, 2231 (1994).

[18] N. C. Handy and A. M. Lee, Chem. Phys. Lett. **252**, 425 (1996).

[19] W. Cencek and W. Kutzelnigg, J. Chem. Phys. **105**, 5878 (1996).

[20] R. Jaquet, W. Cencek, W. Kutzelnigg, and J. Rychlewski, J. Chem. Phys. **108**, 2837 (1998).

[21] R. Prosmiti, O. L. Polyansky, and J. Tennyson, Chem. Phys. Lett. **273**, 107 (1997).

[22] O. L. Polyansky, R. Prosmiti, W. Klopper, and J. Tennyson, Mol. Phys. **98**, 261 (2000).

[23] A. Aguado, O. Roncero, C. Tablero, C. Sanz, and M. Paniagua, J. Chem. Phys. **112**, 1240 (2000).

[24] L. F. Errea, A. Macías, L. Méndez, I. Rabadán, and A. Riera, Phys. Rev. A **65**, 010701(R) (2001).

[25] M. Baer, G. Niedner-Schatteburg, and J. P. Toennies, J. Chem. Phys. **91**, 4169 (1989).

[26] F. O. Ellison, J. Am. Chem. Soc. **85**, 3540 (1963).

[27] R. K. Preston and J. C. Tully, J. Chem. Phys. **54**, 4297 (1971).

[28] M. Baer and H. Nakamura, J. Chem. Phys. **87**, 4651 (1987).

[29] L. Monchick and E. Mason, J. Chem. Phys. **35**, 1676 (1961).

[30] K. H. Kramer and R. B. Bernstein, J. Chem. Phys. **40**, 200 (1964).

[31] T. P. Tsien, G. A. Parker, and R. T. Pack, J. Chem. Phys. **59**, 5373 (1973).

[32] D. Secrest, J. Chem. Phys. **62**, 710 (1975).

[33] J. Morales, A. Diz, E. Deumens, and Y. Öhrn, J. Chem. Phys. **103**, 9968 (1995).

[34] I. Last, M. Gilibert, and M. Baer, J. Chem. Phys. **107**, 1451 (1997).

[35] D. Elizaga, L. F. Errea, J. D. Gorfinkiel, A. Macías, L. Méndez, A. Riera, and A. Rojas, J. Phys. B: At. Mol. Opt. Phys. **33**, 2037 (2000).

[36] M. W. Gealy and B. I. Van Zyl, Phys. Rev. A **36**, 3091 (1987).

[37] L. F. Errea, A. Macías, L. Méndez, I. Rabadán, and A. Riera, Unpublished.

[38] P. S. Krstić, Phys. Rev. A **66**, 042717 (2002).

[39] H. Nakamura, A. Oshaki, and M. Baer, J. Phys. Chem. **90**, 6176 (1986).

[40] A. Ichihara, O. Iwamoto, and R. Janev, J. Phys. B: At. Mol. Opt. Phys. **33**, 4747 (2000).

[41] P. S. Krstić and R. K. Janev, Phys. Rev. A **67**, 022708 (2003).

[42] P. O. Widmark, P. Malmqvist, and B. Roos, Theor. Chim. Acta **77**, 291 (1990).

[43] L. F. Errea, A. Macías, L. Méndez, I. Rabadán, and A. Riera, Int. J. Mol. Sci. **3**, 142 (2002).

[44] J. D. Power, Phil. Soc. Trans. R. Soc **274**, 663 (1973).

[45] A. Macías, L. F. Errea, J. D. Gorfinkiel, L. Méndez, and A. Riera, J. Mol. Struct. (Theochem) **433**, 169 (1998).

[46] L. F. Errea, L. Fernández, A. Macías, L. Méndez, I. Rabadán, and A. Riera, J. Chem. Phys. **121**, 1663 (2004).

[47] A. Macías and A. Riera, Phys. Rep. **81**, 299 (1982).

[48] L. Pauling and E. B. Willson, *Introduction to Quantum Mechanics* (Mc Graw-Hill, New York, 1935).

[49] M. Karplus and R. N. Porter, *Atoms and Molecules* (Bejamin, Menlow Park, 1970).

[50] E. E. Nikitin, Ad. Quan. Chem. **5**, 185 (1970).

[51] L. D. Landau and E. M. Lifshitz, *Quantum Mechanics* (Pergamon, Oxford, 1965).

[52] C. Zener, Proc. R. Soc. London **Ser. A 137**, 696 (1932).

[53] Y. N. Demkov, Sov. Phys. JETP **18**, 138 (1964).

[54] C. A. Mead and D. G. Truhlar, J. Chem. Phys. **77**, 6090 (1982).

[55] M. Baer, Chem. Phys. Lett. **35**, 112 (1975).

[56] M. Baer (CRC Press, Inc. Boca Raton, Florida, 1985), vol. II, p. 232.

[57] L. F. Errea, A. Macías, L. Méndez, I. Rabadán, A. Riera, A. Rojas, and P. Sanz, Phys. Rev. A **63**, 062713 (2001).

[58] F. T. Smith, Phys. Rev. **179**, 111 (1969).

[59] M. Chajia and R. Levine, Phys. Chem. Chem. Phys. **1**, 1205 (1999).

[60] Z. H. Top and M. Baer, Chem. Phys. **25**, 1 (1977).

FIG. 1: Schematic representation of the H_3^+ system in Jacobi coordinates.

FIG. 2: Fixed angle ($\theta = \pi/3$) *ab initio* potential energy contours for the ground $X\ ^1A'$ and first excited $1\ ^1A'$ electronic states of the H_3^+ system.

FIG. 3: (a) *Ab initio* coupling $\partial_R^{\rho,\theta}$ (in a.u.) as a function of R for different values of ρ, and (b) $\partial_\rho^{R,\theta}$ (in a.u.) as a function of ρ for different values of R. These values are for geometries with $\theta = \pi/3$.

FIG. 4: Isocontour plots for the nonadiabatic couplings between the $X\ ^1A'$–$1\ ^1A'$ electronic states of the H_3^+ system for $\theta = \pi/3$. Isocontour lines are plotted for increments of 0.05 a.u. in the value of the coupling, starting with 0.05 a.u. for positive values (solid lines) and −0.05 a.u. for negative values (dashed lines). Panels (a) and (b): $\partial_R^{\rho,\theta}$. Panels (c) and (d): $\partial_\rho^{R,\theta}$. Panels (a) and (c) are *ab initio* calculations while (b) and (d) are the DIM calculations. Solid thick lines mark the *loci* of the corresponding nonadiabatic couplings (see text). Straight dashed-dotted lines divide the configuration (R,ρ)-plane in regions I, II and III [only marked in panel (b)], as discussed in text.

FIG. 5: Isocontour plots of the DIM nonadiabatic $X\ ^1A'$–$1\ ^1A'$ couplings: $\partial_R^{\rho,\theta}$, top row of panels; $\partial_\rho^{R,\theta}$, bottom row of panels. The θ-angles are indicated for each column of panels. We have also drawn the ellipse of Eq. (11) with a thick solid line.

FIG. 6: (a) DIM and (b) *ab initio* residual couplings ${}^{\rm d}\partial_\rho^{R,\theta}$ [Eq. (15)] corresponding to the couplings of Fig. 3(b). Note the different order of magnitude of the residual couplings in both panels.

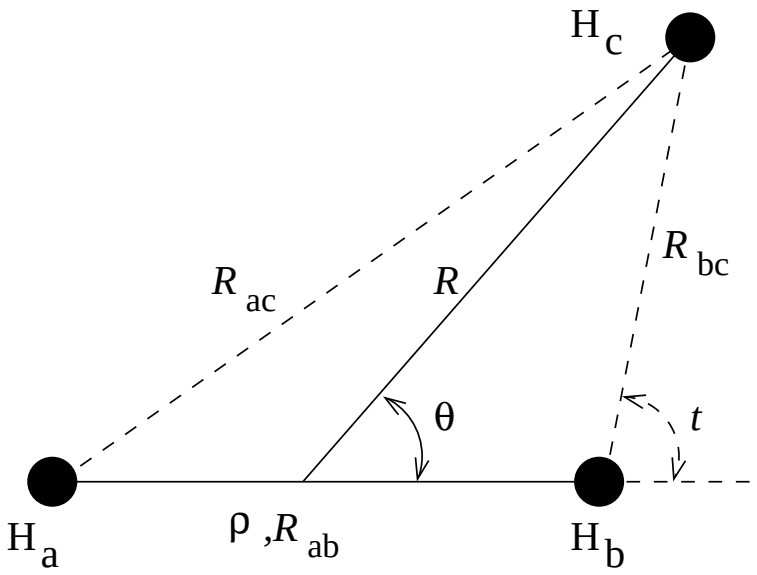

Figure 1, Barragan et al, J. Chem. Phys.

Figure 2, Barragan et al, J. Chem. Phys.

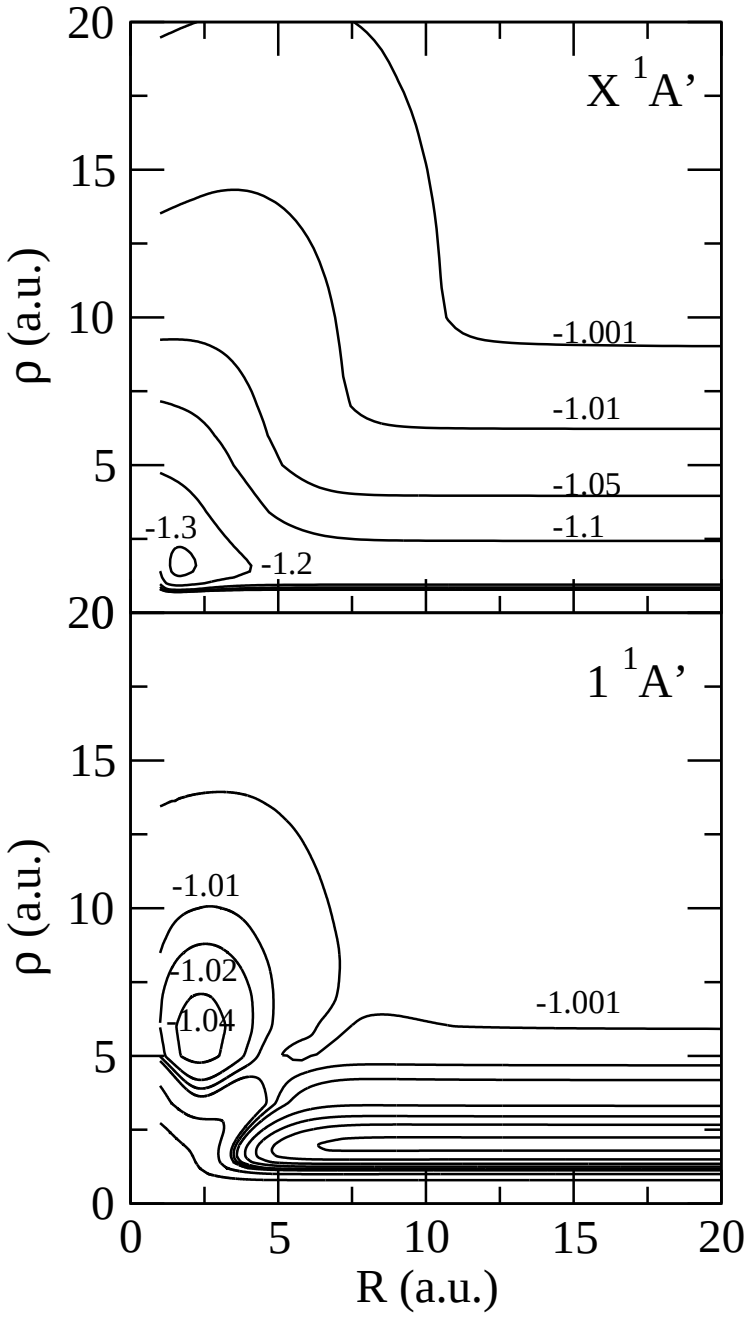

Figure 3, Barragan et al, J. Chem. Phys.

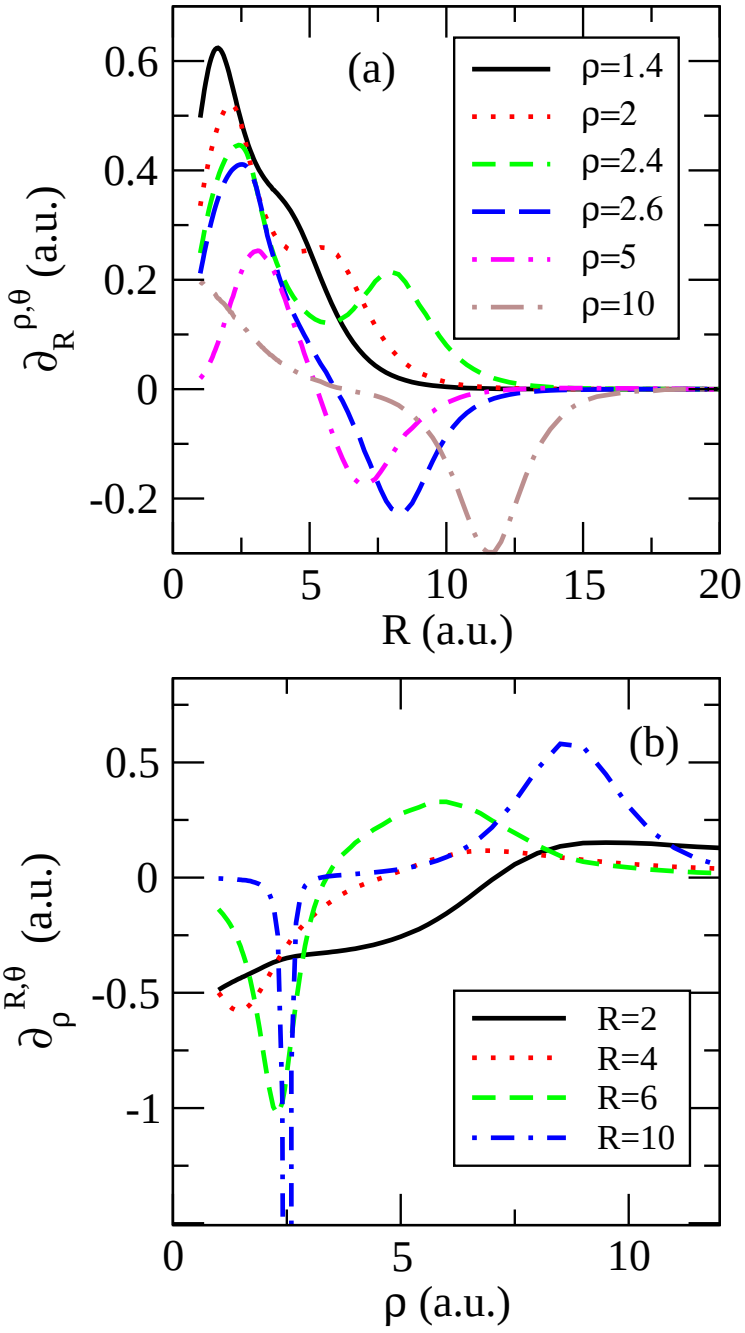

Figure 4, Barragan et al, J. Chem. Phys.

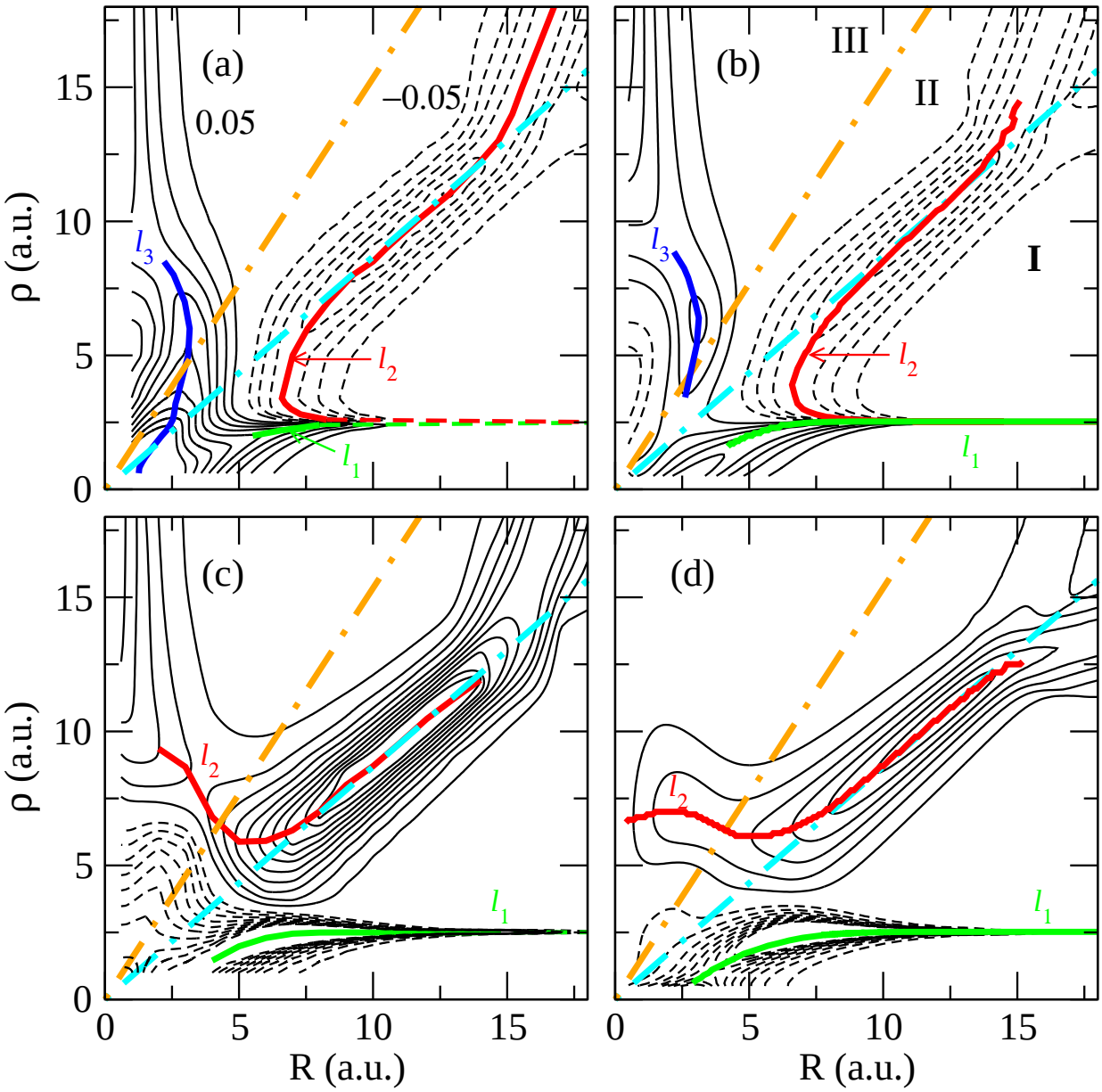

Figure 5, Barragan et al, J. Chem. Phys.

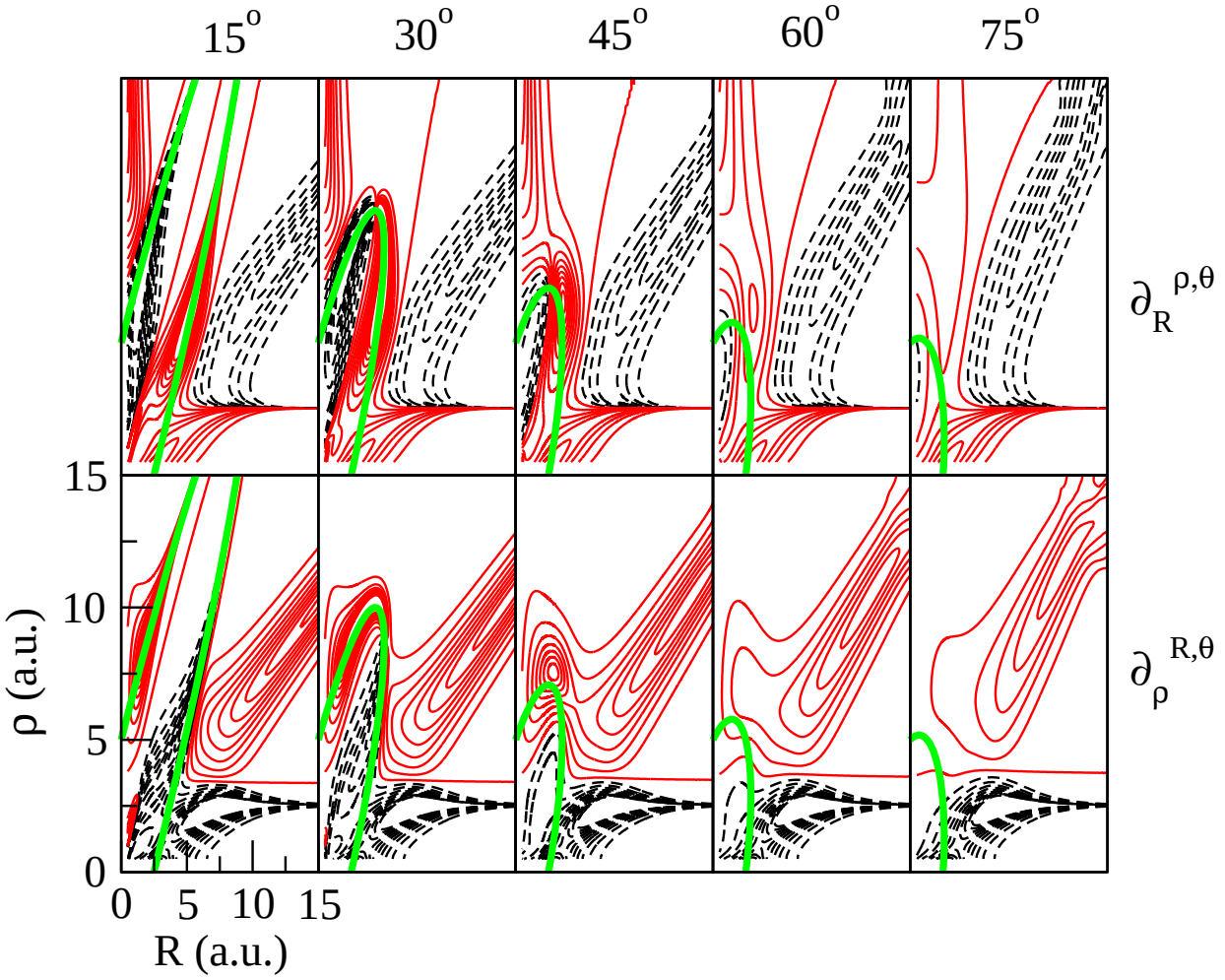

Figure 6, Barragan et al, J. Chem. Phys.